Journal of King Saud University – Computer and Information Sciences (2018) 30, 41–50

King Saud University

Journal of King Saud University – Computer and Information Sciences

www.ksu.edu.sa
www.sciencedirect.com

CT image denoising using locally adaptive shrinkage rule in tetrolet domain

Manoj Kumar, Manoj Diwakar *

Babasaheb Bhimrao Ambedkar University, Lucknow, India

Received 11 December 2015; revised 24 February 2016; accepted 17 March 2016
Available online 31 March 2016

KEYWORDS

Image denoising;
Wavelet transform;
Tetrolet transform;
Shrinkage rule

Abstract In Computed Tomography (CT), image degradation such as noise and detail blurring is one of the universal problems due to hardware restrictions. The problem of noise in CT images can be solved by image denoising. The main aim of image denoising is to reduce the noise as well as preserve the important features such as edges, corners, textures and sharp structures. Due to the large capability of noise suppression in noisy signals according to neighborhood pixels or coefficients, this paper presents a new technique to denoise CT images with edge preservation in tetrolet domain (Haar-type wavelet transform) where a locally adaptive shrinkage rule is performed on high frequency tetrolet coefficients in such a way that noise can be reduced more effectively. The experimental results of the proposed scheme are excellent in terms of noise suppression and structure preservation. The proposed scheme is compared with some standard existing methods where it is observed that performance of the proposed scheme is superior to the existing methods in terms of visual quality, MSE, PSNR and Image Quality Index (IQI).

1. Introduction

CT examination is widely used in medical science for detection of diseases such as lung cancer. Higher radiation dose used for clinical CT scanning may increase the risk of cancer in the patients (Zhoubo et al., 2014). However, it is mentioned in the guidelines of CT scanning that the use of radiation should be as low as reasonably required. But many times, we have to compromise with these guidelines to achieve good quality CT images. On the other-side, low-dose CT imaging may produce a noisy image which degrade the diagnostic performance. Thus, there is a need to develop the techniques which can control the noise in low dose CT scan images.

Various techniques have been investigated for controlling noise in CT scan imaging. Broadly, these techniques can be categorized in three major parts : projection based denoising, iterative reconstruction (IR) based denoising and post processing based image denoising.

Projection based techniques such as projection space denoising with bilateral filtering and CT noise modeling for dose reduction in CT imaging (Manduca et al., 2009) work on raw data or sinogram, where noise filtering is applied on

* Corresponding author.
E-mail address: manoj.diwakar@gmail.com (M. Diwakar).
Peer review under responsibility of King Saud University.

Production and hosting by Elsevier

http://dx.doi.org/10.1016/j.jksuci.2016.03.003

raw data or sinogram and reconstructed image comes in the form of denoised image. Many iterative reconstruction approaches for noise suppression in CT have also been investigated, for example, ordered subset reconstruction for X-ray CT scan (Beekman and Kamphuis, 2001) that optimizes statistical objective functions. Iterative reconstruction techniques have an advantage of using noise statistics directly in the projections during the reconstruction process, the disadvantage, however, is the high computational cost. Post processing based methods can denoise directly to the reconstructed CT images by applying linear or nonlinear filters (Motwani et al., 2004). Several linear or nonlinear filtering methods for noise reduction in the projection data have been proposed. Linear filters such as Wiener filter (Li and Zhang, 2010; Naimi et al., 2015) in the wavelet domain gives optimal results when the signal distortion is estimated by Gaussian approximation and the accuracy is measured by calculating Mean Square Error (MSE). Most of the techniques like bilateral filtering (Durand and Dorsey, 2002; Manduca et al., 2009), total variation denoising (Chambolle, 2004; Goldstein and Osher, 2009), nonlocal means (NLM) denoising (Buades et al., 2005), local linear SURE based edge-preserving image filtering (LLSURE) (Qiu et al., 2013) and K-singular value decomposition (K-SVD) algorithm (Aharon et al., 2006) take an advantage of statistical properties of objects in image space and preserve clinical structures such as sharp edges, similarities between neighboring pixels, etc. In transform-domain denoising techniques, the input data are decomposed into its scale-space representation (Mallat, 1989). Various thresholding techniques for noise reduction have been introduced with wavelet such as efficient image denoising method based on a new adaptive wavelet packet thresholding function (Fathi and Naghsh-Nilchi, 1989), ideal spatial adaptation via wavelet shrinkage (Chang et al., 2000), SURE-LET approach for image denoising (Thierry and Florian, 2007), etc. For CT image denoising, selection of a threshold value is a cumbersome task for edge preservation and noise suppression. By selecting a small threshold value, the resultant image may left noisy while large threshold value may produce blurring on the edges of resultant image. To deal with this situation, an appropriate algorithm is to be selected to estimate a threshold value. Three major algorithms to estimate threshold value are VISUShrink, SUREShrink and BayesShrink. VISUShrink (Donoho and Johnstone, 1994) is non-adaptive universal threshold, which depends only on the number of samples and known for finding smoothed images. Its threshold choice can be large due to its dependence on the number of pixels in the images. From literature, it can be observed that threshold estimation of VISUShrink tends to over-smooth the signal while SUREShrink (Donoho, 2010) uses a hybrid of the universal and the SURE [Stein's Unbiased Risk Estimator] thresholds, and performs better than VISUShrink. BayesShrink (Abramovitch et al., 1998) minimizes the Bayes' risk estimator function assuming generalized Gaussian approximation and thus finds adaptive threshold value. In most of the cases, BayesShrink provides better outcomes in comparison to both VISUShrink and SUREShrink. Thresholding is one of the strategies to clean the pixels or images. In wavelet based thresholding, small wavelet coefficients in high frequency bands are removed and large wavelet coefficients are preserved. Hard and soft thresholding are very popular methods for thresholding. In hard thresholding (Donoho, 2010), each coefficient value is compared with estimated threshold value and values less than threshold are replaced by zero. In soft thresholding (Prakash and Khare, 2014), the replacement process is same as in hard thresholding, additionally rest of coefficients are modified by subtracting threshold value from those coefficients. Comparing the two, Soft thresholding gives better performance for visual appearance of images. Due to hard thresholding, image artifacts may be generated near the edges on denoised CT images. Soft thresholding has a limitation with large coefficient values which may not be good for more sophisticated CT images. Other thresholding schemes have also been proposed, which take the advantages of both soft and hard thresholding. Some well-known shrinkage rules are hyperbola function (Vidakovic, 1998), firm thresholding (Gao and Bruce, 1997), garrote thresholding (Gao, 1998) and SCAD thresholding (Antoniadis and Fan, 2001).

Recently, some researchers extended the idea of shrinkage with geometric wavelets methods (Krommweh, 2010) such as ridgelet, curvelets, contourlets, directionlet and tetrolet. CT image denoising is a challenging task because of finding correct noise variation, relationship between coefficients and achieving an optimal tradeoff between denoising and blurring or artifacts. To overcome these challenges, we propose a method for CT image denoising based on the variation of neighborhood pixels or coefficients.

This paper is organized as follows. In Section 2, a brief introduction of tetrolet transform is described. In Section 3, we describe the proposed methodology for CT image denoising where a locally adaptive shrinkage rule is performed in tetrolet transform. In Section 4, we describe the experimental results and compare with some existing denoising methods. Finally, conclusions are drawn in Section 5.

2. Tetrolet transform

The idea of tetrolet transform comes from a famous computer game 'Tetris', where five geometric patterns (as shown in Fig. 1 (a)) are used with rotation and reflection properties (Krommweh, 2010). These geometric patterns are known as tetrominoes. Tetrolet transform is a powerful tool for signal and image processing tasks because of local enhancement through tetrominoes, multi-resolution analysis, sub-banding and localization in both frequency and time domain. All the tetrominoes are connected with a four equal sized squares. In tetrolet transform, an image $X[i,j]_{i,j=1}^{N}$ with $N = 2^P,\ P \in N$ is divided into 4×4 blocks. Each block is covered with any four free tetrominoes, which is responsible for enhancing the local structure using properties of rotations and reflections. These four tetrominoes (I_o, I_1, I_2, I_3) are mapped in a unique order (0, 1, 2, 3) by applying bijective mapping (L) with their corresponding order. For each tetromino subset (I_v), the discrete basis functions (Krommweh, 2010) are defined as follows:

$$\phi_{I_v}[i,j] := \begin{cases} 1/2; & (i,j) \in I_v \\ 0; & \text{otherwise} \end{cases}$$

$$\psi^l_{I_v}[i,j] := \begin{cases} \in [l, L(i,j)]; & (i,j) \in I_v \\ 0; & \text{otherwise} \end{cases}$$

for $l = 1, 2, 3$, $\psi^l_{I_v}$ represents tetrolets and ϕ_{I_v} is scaling function. Haar wavelet transform matrix W has four fixed 2×2

squares with 117 solution for disjoint covering of a 4×4 board.

$$W = (\in [m,n])_{m,n=0}^{3} = \frac{1}{2}\begin{pmatrix} 1 & 1 & 1 & 1 \\ 1 & 1 & -1 & -1 \\ 1 & -1 & 1 & -1 \\ 1 & -1 & -1 & 1 \end{pmatrix}$$

There are 117 kinds of tilings for covering of a 4×4 block with any four tetrominoes (Jain and Tyagi, 2015). Fig. 1(b) represents one of the covering from 117 kinds of tilings and Fig. 1(c) represents its local structure.

3. Proposed methodology

Generally, the distribution of noise in CT images follows the Poisson distribution due to statistical fluctuations on X-ray projected data (Rabbani et al., 2009). However, different reconstruction algorithms can change the distribution of noise model. Thus by Central Limit Theorem (CLT), the noise can be best modeled by Gaussian distribution (Rabbani, 2009; Ali and Sukanesh, 2011; Zhu et al., 2012). The CLT in CT images can be obtained by adding values from many different projections into each voxel of CT images (Hashemi et al., 2015; Borsdorf et al., 2008; Naimi et al., 2015). With the assumption that the CT images are corrupted by Gaussian noise with zero mean and different variances, the scheme is proposed using locally adaptive shrinkage rule in tetrolet domain.

Let, the noisy image $X(i,j)$ be expressed as:

$$X(i,j) = Y(i,j) + \eta(i,j) \tag{1}$$

where, η is an additive noise, Y is noiseless image. The block diagram of the proposed scheme is shown in Fig. 2. For denoising of noisy CT scanned images, tetrolet transform plays a major role to enhance the local information of an image because of multi-scale geometric property.

In our proposed scheme, tetrolet transform is used to decompose input noisy CT image into low (LL) and high (LH, HL, HH) frequency subbands. Generally, physicians prefer original noisy images more willingly in comparison to smooth images for more sophisticated CT images. Therefore, low frequency tetrolet subbands are not processed. The perfect optimization for estimating a threshold value is an almost impossible task for image denoising. Thus as an alternative, an iterative method (Gupta et al., 2014) is used to get an

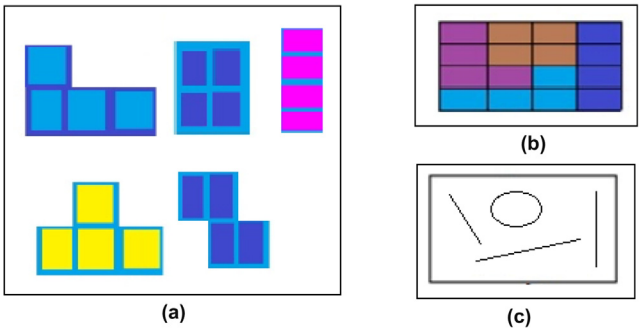

Figure 1 Tetromeno patterns with example. (a) Five tetromeno patterns. (b) One of the disjoint covering from 117 kind of tilings. (c) Corresponding local structure of (b).

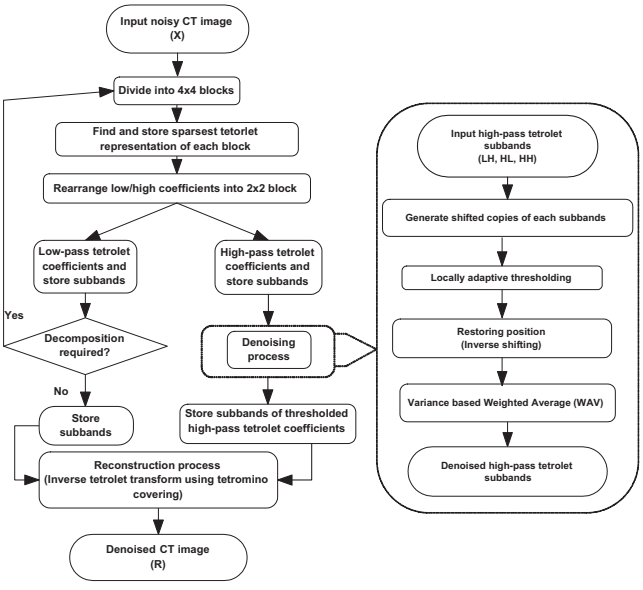

Figure 2 Proposed scheme.

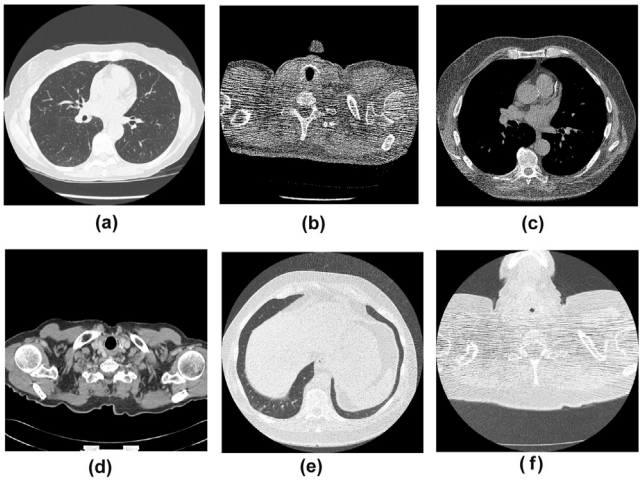

Figure 3 Original CT image data set.

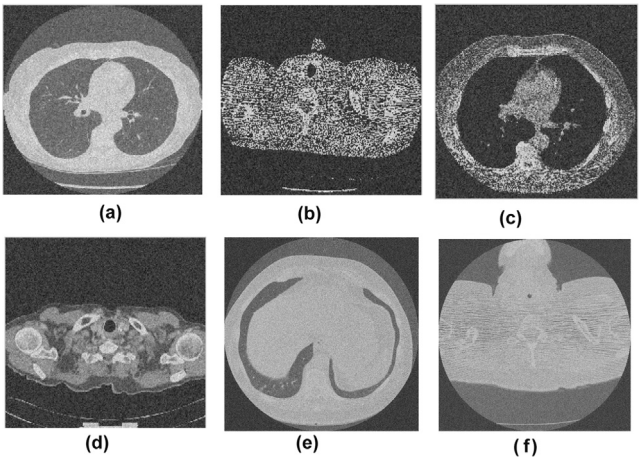

Figure 4 Noisy CT image data set $\sigma = 20$.

Table 1 Average correlation values between multiple thresholded high frequency subbands.

L	X^{LH}						X^{HL}						X^{HH}					
	CT1	CT2	CT3	CT4	CT5	CT6	CT1	CT2	CT3	CT4	CT5	CT6	CT1	CT2	CT3	CT4	CT5	CT6
L = 1	0.9996	0.9934	0.9826	0.9656	0.9967	0.9989	0.9843	0.9992	0.9965	0.9892	0.9971	0.9992	0.9787	0.9692	0.9856	0.9801	0.9985	0.9994
L = 2	0.9732	0.9810	0.9721	0.9591	0.9741	0.9641	0.9571	0.9843	0.9669	0.9801	0.9793	0.9635	0.9619	0.9491	0.9624	0.9612	0.9703	0.9667
L = 3	0.9510	0.9583	0.9634	0.9310	0.9545	0.9431	0.9391	0.9623	0.9503	0.9511	0.9572	0.9410	0.9592	0.9312	0.9478	0.9598	0.9458	0.9498
L = 4	0.9497	0.9304	0.9331	0.9006	0.9365	0.9211	0.9131	0.9378	0.9395	0.9402	0.9476	0.9351	0.9271	0.9020	0.9378	0.9327	0.9309	0.9274
L = 5	0.9158	0.9043	0.9163	0.8912	0.9019	0.9143	0.9023	0.9191	0.9112	0.9229	0.9086	0.9071	0.9067	0.8932	0.9106	0.9208	0.9069	0.9104

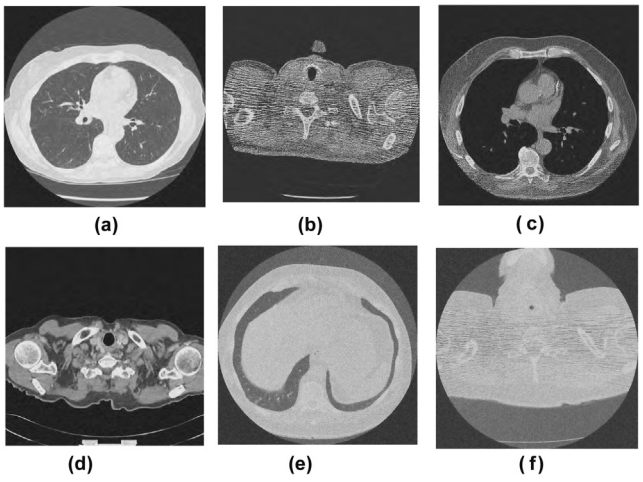

Figure 5 Results of LLSURE.

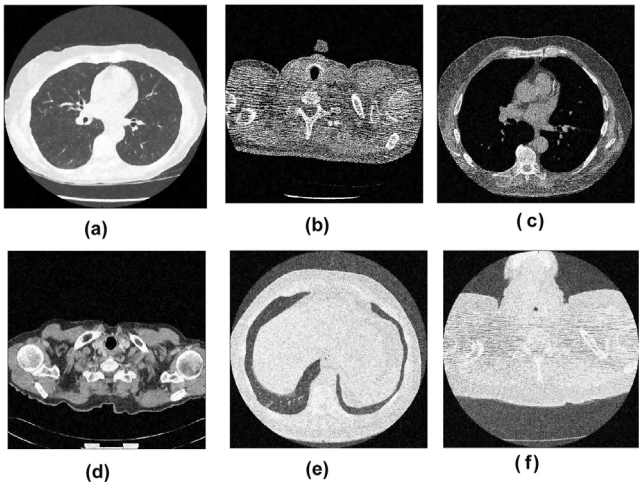

Figure 6 Results of Bilateral filtering.

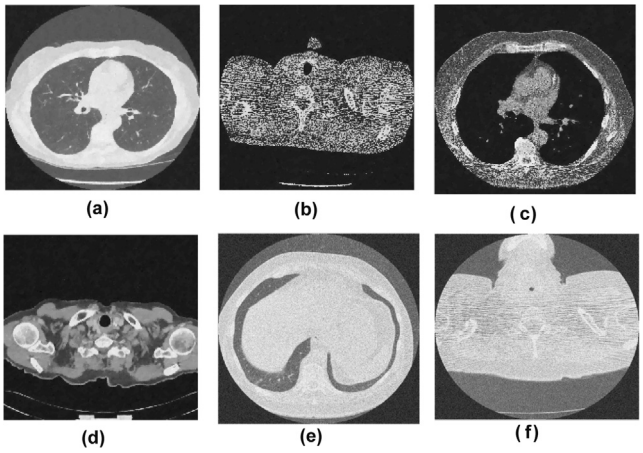

Figure 7 Results of total variation denoising.

optimum thresholded value for each coefficient. To accomplish this, we made several high-frequency tetrolet subbands by shifting the coefficient position in the direction of x- and/or y-axis circularly which are known as shifted copies of respective high-frequency tetrolet subbands. These shifted high frequency subbands are thresholded separately by applying locally adaptive shrinkage rule using estimated threshold value and averaged to get final denoised coefficients.

In our proposed scheme, BayesShrink method is used to estimate the threshold value. BayesShrink is a mathematical framework where it is assumed that each high frequency subbands of tetrolet coefficients are generalized by Gaussian distribution to estimate the threshold value that minimizes the Bayesian risk. To denoise high frequency subbands, a threshold value is estimated and thresholding is performed. The threshold value can be estimated as,

$$\lambda = \frac{\sigma_\eta^2}{\sigma_Y} \tag{2}$$

where the noise variance (σ_η^2) can be estimated using robust median estimator method (Borsdorf et al., 2008) and defined as:

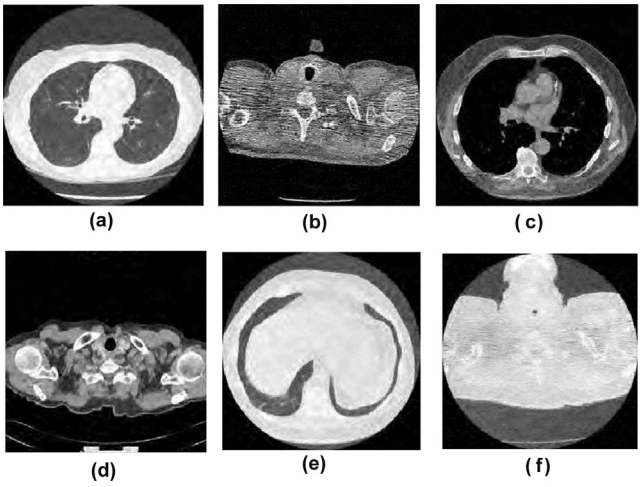

Figure 8 Results of SURELET.

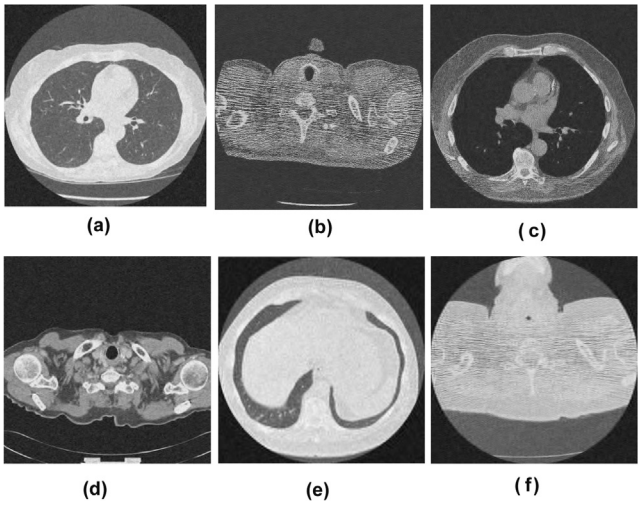

Figure 9 Results of Bayes thresholding.

$$\sigma_\eta^2 = \left[\frac{median(|X(i,j)|)}{0.6745}\right]^2 \tag{3}$$

and variance σ_W^2 of noiseless image can be extracted as,

$$\sigma_Y^2 = max\left(\sigma_X^2 - \sigma_\eta^2, 0\right) \tag{4}$$

where $\sigma_X^2 = \frac{1}{w}\sum_{i=1}^{w} X_i^2$ and w represents the number of pixels in a selected block.

In our proposed scheme, a thresholding shrinkage rule (Gao and Bruce, 1997) is used to denoise high frequency tetrolet subbands which helps to avoid the limitations of both hard and soft thresholding. This function also helps to minimize the overall mean-squared error. The thresholding function can be expressed as:

$$\hat{X}' := \begin{cases} X, & \text{if } |X| > \lambda_2 \\ sign(X)\frac{\lambda_2(|X|-\lambda_1)}{\lambda_2-\lambda_1}, & \text{if } \lambda_1 < |X| \leqslant \lambda_2 \\ 0, & \text{Otherwise} \end{cases} \tag{5}$$

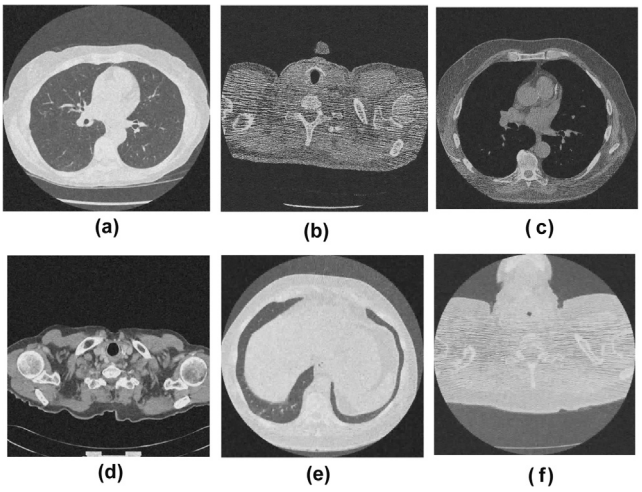

Figure 10 Results of biorthogonal wavelet thresholding.

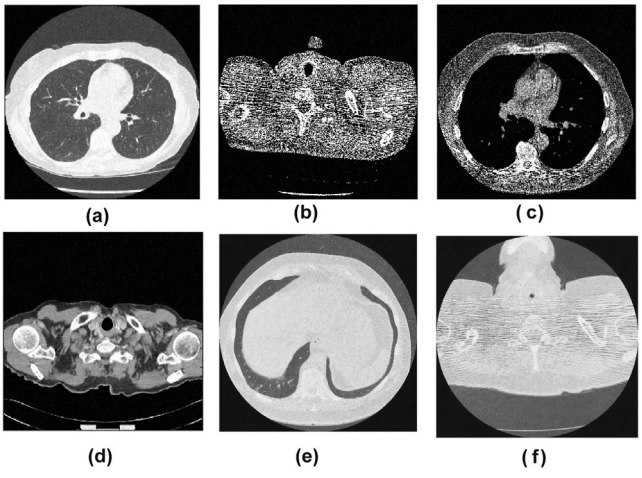

Figure 11 Results of proposed scheme.

After thresholding process, all shifted copies of high frequency tetrolet subbands are restored by shifting coefficients into their original position and patch wise variance based weighted average is performed to get final thresholded high frequency tetrolet subbands. Finally, inverse tetrolet decomposition is performed to obtain final denoised CT image.

Our proposed method consist the following steps:

Step 1: Apply tetrolet decomposition on noisy input CT image to obtain low and high frequency subbands as below:

(a) Divide the image into 4×4 blocks.

(b) Set the decomposition level and tetromino covering values (by, 117).

(c) Find and store sparsest tetrolet representation of each block.

(d) Rearrange low/high coefficients into 2×2 blocks and obtain low and high frequency subbands.

(e) Extraction of further decomposition on low frequency subband:

- For each level, low frequency subbands are decomposed. Decomposed subbands are known as child node for respective parent node.
- Calculate the entropy as a cost function (Fathi and Naghsh-Nilchi, 1989) of each child nodes as well as parent nodes.
- In top down approach manner, check the cost value. If the cost of parent node is greater than total cost of child nodes; Continue further decomposition. Otherwise; Stop decomposition and eliminate children nodes.

Step 2: Prepare k number of shifted copies of high frequency tetrolet subbands by shifting the coefficient positions in the direction of the x- and/or y-axis circularly.

$$X'(i,j)_{s^{\gamma}} = circular\_shift\{X(i,j)_s, [i_{shift}, j_{shift}]\} \tag{6}$$

where $\gamma = 1 \ldots k$, the value of k depends on the length of respective high frequency tetrolet subband.

Step 3: For each decomposition level (L):

(a) Calculate local noise variance using Eq. (3)

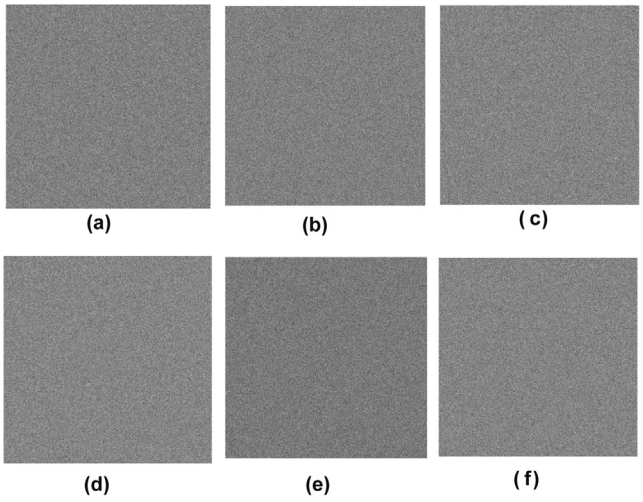

Figure 12 Difference between original and noisy image.

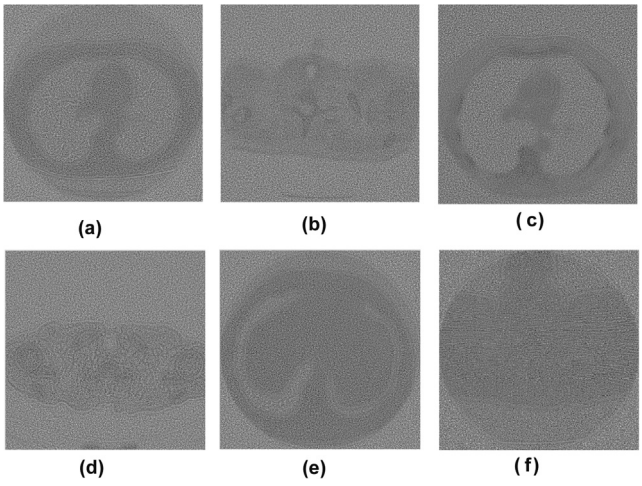

Figure 14 Difference between original and bilateral filtered image.

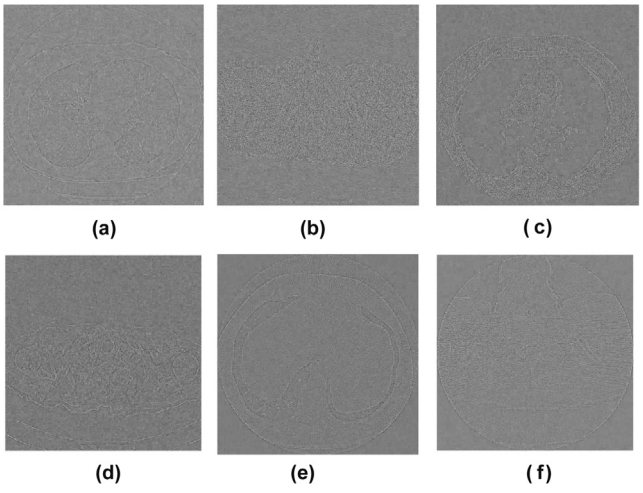

Figure 13 Difference between original and LLSURE filtered image.

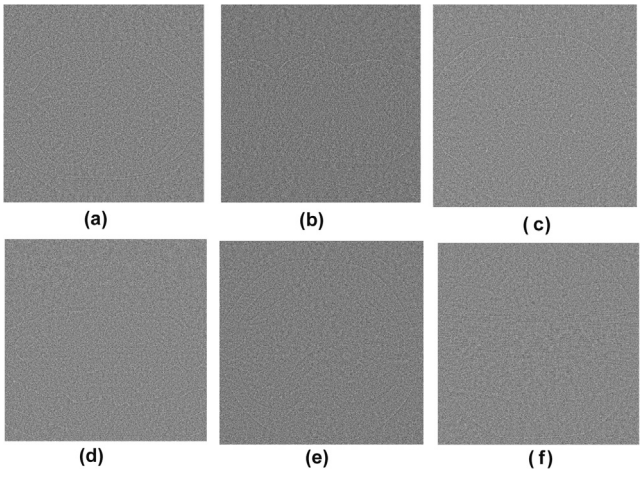

Figure 15 Difference between original and total variation denoised image.

(b) For each tetrolet coefficients in each subband (s):
(i) Compute threshold value λ_1 using Eq. (2)
(ii) Compute threshold value λ_2, by setting $\lambda_2 = 0.9 \cdot \lambda_1$
(iii) Apply shrinkage rule using Eq. (5)

Step 4: After thresholding on each subband, perform the inverse shift. The resulting thresholded high frequency tetrolet coefficients $(\widehat{X}'(i,j)_{s^{\vec{\gamma}}})$ are shifted back to the original position and the multiple high frequency tetrolet modified subbands are stored.

$$X''(i,j)_{s^{\vec{\gamma}}} = circular\_shift\{\widehat{X}'(i,j)_{s^{\vec{\gamma}}}, [-i_{shift}, -j_{shift}]\} \tag{7}$$

Step 5: To get final denoised high frequency tetrolet subbands, perform patch wise variance based weighted average on multiple high frequency tetrolet modified subbands, as given below (Jain and Tyagi, 2015):

$$\widehat{X}(i,j)_s = \sum_{\gamma=1}^{k} \alpha_{s^{\vec{\gamma}}} \cdot X''(i,j)_{s^{\vec{\gamma}}} \tag{8}$$

where $\alpha_{s^{\vec{\gamma}}} = \frac{var^{-1}(X''_{w,s^{\vec{\gamma}}})}{\sum_{\gamma=1}^{k} var^{-1}(X''_{w,s^{\vec{\gamma}}})}$, $var^{-1}(\cdot)$ represents inverse of the variance, $\hat{X}(i,j)_s$ is the final thresholded value for the coefficient at position (i,j) in the subband s and w is local neighborhood which is used to calculate the local variance.

Step 6: Perform the tetrolet reconstruction, to get the final denoised CT image.

4. Experimental results and discussion

The experimental evaluation is performed on noisy CT images with size 512x512. The CT scanned test images shown in Fig. 3 (a–f) are obtained from public access database (https://eddie.via.cornell.edu/cgibin/datac/logon.cgi). The proposed image denoising scheme is applied to all test images corrupted by additive Gaussian white noise at four different noise levels (σ): 10, 20, 30, and 40. Fig. 3(a–f) is considered as CT image 1, 2, 3, 4, 5 and 6 respectively. Fig. 4(a–f) shows noisy test image data set with $(\sigma) = 20$.

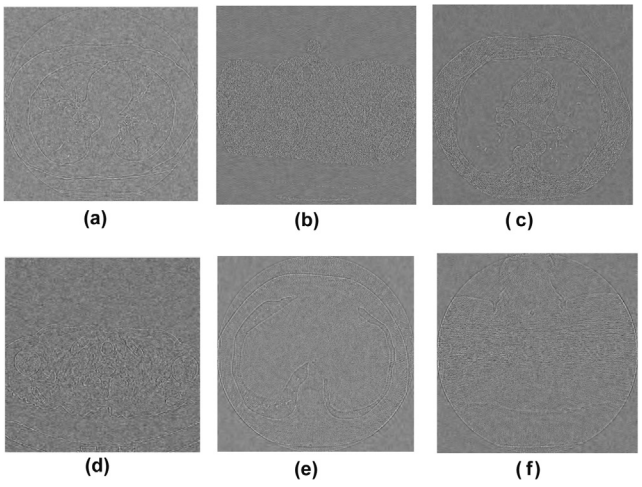

Figure 16 Difference between original and SURELET filtered image.

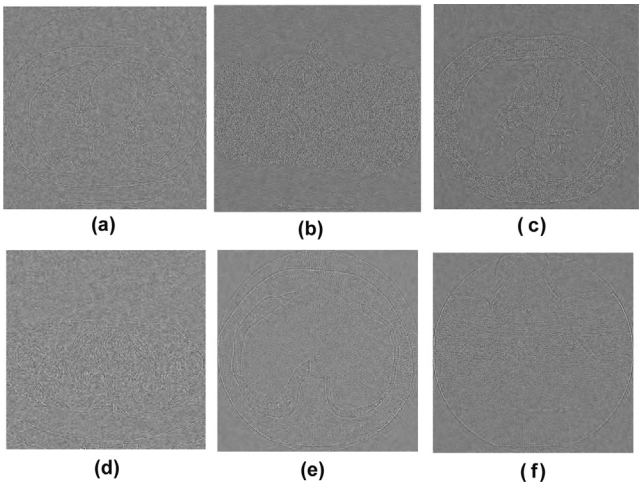

Figure 17 Difference between original and Bayes denoised image.

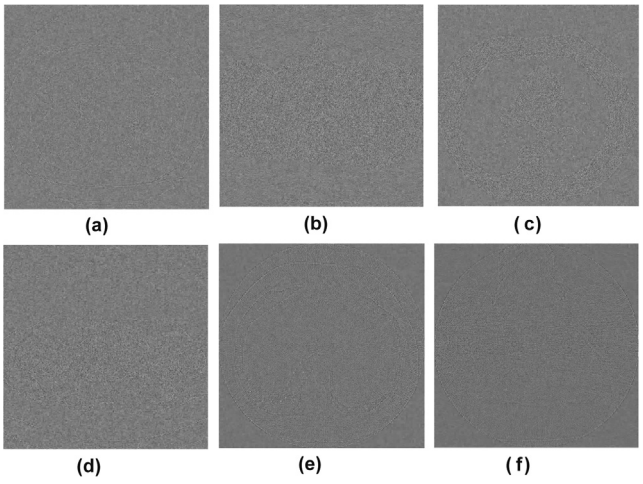

Figure 18 Difference between original and biorthogonal wavelet based denoised image.

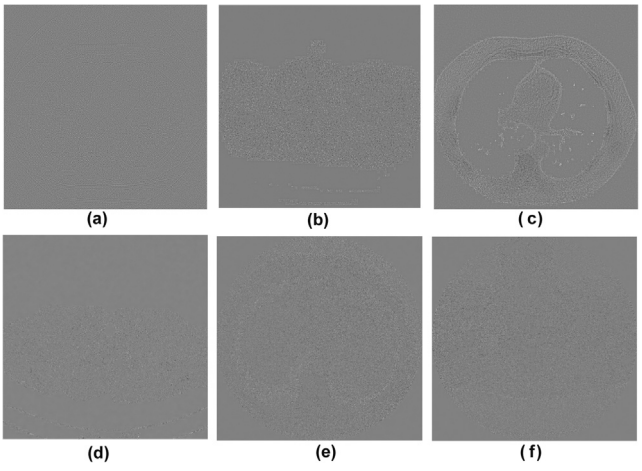

Figure 19 Difference between original and proposed scheme based denoised image.

Table 2 MSE, PSNR and IQI of CT denoised images.

Image	σ	MSE				PSNR				IQI			
		10	20	30	40	10	20	30	40	10	20	30	40
CT1	LLSURE (Qiu et al., 2013)	40.20	116.17	205.15	281.24	32.09	27.45	25.01	23.64	0.9968	0.9019	0.8864	0.8670
	Bilateral (Durand and Dorsey, 2002)	50.35	102.58	154.19	231.24	31.11	28.02	26.25	24.49	0.9952	0.9174	0.8972	0.8711
	TV (Goldstein and Osher, 2009)	40.55	96.17	145.90	258.27	32.05	28.30	26.49	24.01	0.9976	0.9175	0.8831	0.8540
	SURELET (Thierry and Florian, 2007)	46.99	102.82	158.88	227.02	31.41	28.01	26.12	24.57	0.9951	0.9168	**0.8961**	0.8702
	Bayes (Chang et al., 2000)	39.27	96.62	145.23	258.27	32.19	28.28	26.51	24.01	0.9971	0.9147	0.8832	0.8521
	Bior (Prakash and Khare, 2014)	38.91	93.77	147.59	239.92	32.23	28.41	26.54	24.33	0.9973	0.9139	0.8812	0.8510
	Proposed	**34.76**	**88.32**	**119.42**	**207.05**	**32.72**	**28.67**	**27.36**	**24.97**	**0.9993**	**0.9298**	0.8949	**0.8841**
CT2	LLSURE (Qiu et al., 2013)	39.90	95.73	155.98	258.27	32.12	28.32	26.20	24.01	0.9971	0.9028	0.8953	0.8669
	Bilateral (Durand and Dorsey, 2002)	44.06	**78.17**	153.13	289.78	31.69	**29.20**	26.28	23.51	0.9975	**0.9198**	0.8721	0.8611
	TV (Goldstein and Osher, 2009)	40.65	92.27	145.57	235.00	32.04	28.48	26.50	24.42	0.9973	0.9061	0.8801	0.8506
	SURELET (Thierry and Florian, 2007)	50.82	100.24	155.62	219.72	31.07	28.12	26.21	24.71	0.9952	0.9168	0.8962	0.8712
	Bayes (Chang et al., 2000)	40.18	96.40	146.58	253.55	32.09	28.29	26.47	24.09	0.9976	0.9154	0.8851	0.8552
	Bior (Prakash and Khare, 2014)	39.09	100.01	152.08	241.03	32.21	28.13	26.39	24.31	0.9961	0.9148	0.8863	0.8521
	Proposed	**33.57**	80.18	**123.90**	**207.52**	**32.87**	29.09	**27.20**	**24.96**	**0.9993**	0.9081	**0.8999**	**0.8875**
CT3	LLSURE (Qiu et al., 2013)	51.53	100.01	151.73	252.39	31.01	28.13	26.32	24.11	0.9941	0.8801	0.8781	0.8649
	Bilateral (Durand and Dorsey, 2002)	49.09	80.55	152.78	266.73	31.22	29.07	26.29	23.87	0.9979	0.9080	0.8832	0.8642
	TV (Goldstein and Osher, 2009)	**40.18**	102.82	152.78	258.27	**32.09**	28.01	26.29	24.01	**0.9984**	0.8960	0.8728	0.8572
	SURELET (Thierry and Florian, 2007)	46.99	81.29	125.62	210.90	31.41	29.03	27.14	24.89	0.9950	0.8920	0.8705	0.8613
	Bayes (Chang et al., 2000)	42.08	98.19	144.90	235.54	31.89	28.21	26.52	24.41	0.9947	0.9073	0.8837	0.8609
	Bior (Prakash and Khare, 2014)	43.15	94.20	133.68	225.98	31.78	28.39	26.87	24.59	0.9933	0.9061	0.8828	0.8660
	Proposed	40.27	**73.29**	**125.04**	**207.05**	32.08	**29.48**	**27.16**	**24.97**	0.9961	**0.9089**	**0.8879**	**0.8663**
CT4	LLSURE (Qiu et al., 2013)	59.44	102.82	159.61	230.18	30.39	28.01	26.10	24.51	0.9942	0.8998	0.8709	0.8553
	Bilateral (Durand and Dorsey, 2002)	**43.15**	86.11	155.62	258.27	**31.78**	28.78	26.21	24.01	**0.9981**	0.9031	0.8789	0.8601
	TV (Goldstein and Osher, 2009)	56.37	100.94	141.93	232.85	30.62	28.09	26.61	24.46	0.9962	0.8914	0.8682	0.8565
	SURELET (Thierry and Florian, 2007)	51.53	102.11	154.55	246.64	31.01	28.04	26.24	24.21	0.9953	0.9012	0.8869	0.8659
	Bayes (Chang et al., 2000)	55.09	92.48	147.25	244.38	30.72	28.47	26.45	24.25	0.9976	0.9023	0.8843	0.8636
	Bior (Prakash and Khare, 2014)	52.49	89.55	144.57	225.98	30.93	28.61	26.53	24.59	0.9978	0.9043	0.8813	0.8661
	Proposed	46.78	**83.96**	**139.66**	**216.31**	31.43	**28.89**	**26.68**	**24.78**	0.9979	**0.9059**	**0.8892**	**0.8693**
CT5	LLSURE (Qiu et al., 2013)	44.88	92.27	140.95	268.58	31.61	28.48	26.64	23.84	0.9971	0.8812	0.8633	0.8567
	Bilateral (Durand and Dorsey, 2002)	50.24	103.53	196.82	268.28	31.12	27.98	25.19	23.91	0.9934	0.8966	0.8712	0.8533
	TV (Goldstein and Osher, 2009)	55.09	100.48	151.73	260.66	30.72	28.11	26.32	23.97	0.9932	0.8734	0.8609	0.8598
	SURELET (Thierry and Florian, 2007)	49.21	95.95	138.06	249.50	31.21	28.31	26.73	24.16	0.9953	0.9012	0.8769	0.8619
	Bayes (Chang et al., 2000)	44.47	86.71	132.15	246.64	31.65	28.75	26.92	24.21	0.9960	0.8912	0.8883	0.8610
	Bior (Prakash and Khare, 2014)	44.06	89.75	**131.54**	241.03	31.69	28.60	**26.94**	24.31	0.9967	0.8971	**0.8895**	0.8601
	Proposed	**41.69**	**85.91**	133.37	**237.72**	**31.93**	**28.79**	26.88	**24.37**	**0.9979**	**0.9097**	0.8812	**0.8625**
CT6	LLSURE (Qiu et al., 2013)	50.35	85.52	147.59	286.47	31.11	28.81	26.44	23.56	0.9965	0.8909	0.8616	0.8407
	Bilateral (Durand and Dorsey, 2002)	47.98	82.42	137.42	276.74	31.32	28.97	26.75	23.71	0.9943	0.9078	0.8702	0.8653
	TV (Goldstein and Osher, 2009)	39.72	**81.67**	155.62	239.92	32.14	**29.01**	26.21	24.33	0.9961	**0.9117**	0.8714	0.8575
	SURELET (Thierry and Florian, 2007)	48.09	92.91	140.30	221.86	31.31	28.45	26.66	24.67	0.9948	0.9013	0.8709	0.8617
	Bayes (Chang et al., 2000)	49.09	87.51	144.90	239.37	31.22	28.71	26.52	24.34	0.9977	0.9064	0.8811	0.8672
	Bior (Prakash and Khare, 2014)	49.66	88.12	138.06	231.24	31.17	28.68	26.73	24.49	0.9971	0.9001	0.8898	0.8688
	Proposed	**38.91**	88.32	**135.54**	**219.82**	**32.23**	28.67	**26.81**	**24.71**	**0.9971**	0.9108	**0.8903**	**0.8691**

4.1. Experimental evaluation

With the motivation that in most of the cases, denoising is dependent on the neighborhood pixels or coefficients, our scheme is designed where high frequency tetrolet coefficients are thresholded by changing neighborhood coefficients using circular shifting and multiple thresholded high frequency subbands are obtained as discussed in proposed methodology

section. In our proposed scheme, two threshold values (λ_1 and λ_2) are used in thresholding function. The threshold value (λ_1) can be obtained from Eq. (2). Another threshold value (λ_2) is used to provide less sensitivity for small variations in the data and also for smaller overall mean-squared error (Minasyan et al., 2006). The value of (λ_2) should be between zero to λ_1. Here all experimental results are obtained by setting the threshold value (λ_2) as $\lambda_2 = 0.9\lambda_1$. The results may slightly vary by setting different values of λ_2. The variation between multiple thresholded high frequency subbands can be observed by correlation values. Table 1 shows the obtained average correlation values between multiple thresholded high frequency subbands ($\sigma = 20$).

To achieve maximum edge preserving and effective noise reduction, patch wise variance based weighted average is performed on multiple thresholded high frequency subbands where the patch size is used as 3×3. Using inverse tetrolet decomposition, final denoised image is obtained.

4.2. Performance evaluation

The performance of CT image denoising schemes can be measured using MSE, PSNR and Image Quality Index (IQI).

For input image (X) and denoised image (R), the IQI can be defined as:

$$\mathrm{IQI} = \frac{4\sigma_{XR}\overline{X}\,\overline{R}}{(\sigma_X^2 + \sigma_R^2)\left[(\overline{X})^2 + (\overline{R})^2\right]} \tag{9}$$

where,
$\overline{X} = \frac{1}{N}\sum_{i=1}^{N} X_i$, $\overline{R} = \frac{1}{N}\sum_{i=1}^{N} R_i$, $\sigma_X^2 = \frac{1}{N-1}\sum_{i=1}^{N}(X_i - \overline{X})^2$, $\sigma_R^2 = \frac{1}{N-1}\sum_{i=1}^{N}(R_i - \overline{R})^2$ and $\sigma_{XR} = \frac{1}{N-1}\sum_{i=1}^{N}(X_i - \overline{X})(R_i - \overline{R})$.

The quality of image index range lies between 1 and -1. The best value 1 represents an identical value of input image pixel and denoised image pixel. The lowest value -1 shows that the pixel values are uncorrelated.

Peak Signal-to-Noise Ratio (PSNR) is an important factor to evaluate denoising performance. The higher PSNR values represent more similarity between the denoised and original images. For input image (X) and denoised image (R), the PSNR is expressed as:

$$PSNR = 10 \times \log_{10}\left(\frac{255\times 255}{MSE}\right) \tag{10}$$

where, Mean Square Error (MSE) is defined as

$$MSE = \frac{1}{mn}\sum_{i=0}^{m-1}\sum_{j=0}^{n-1}[X(i,j) - R(i,j)]^2$$

4.3. Comparisons

To validate the superiority of the proposed scheme, its performance is compared in terms of visual quality, MSE, PSNR and Image Quality Index (IQI) of the denoised images using some standard existing methods. For strong comparison, both wavelet and non-wavelet based existing standard methods are used. The existing methods used for comparison are LLSURE (Qiu et al., 2013), Bilateral filtering (Durand and Dorsey, 2002), Total variation (Goldstein and Osher, 2009), SURELET (Thierry and Florian, 2007), wavelet based Bayes thresholding using Daubechies 8 (DB8) (Chang et al., 2000) and medical image denoising based on soft thresholding using bi-orthogonal 1.3 (bior 1.3) multiscale wavelet transform (Prakash and Khare, 2014).

Figs. 5–11 are showing the results of LLSURE (Qiu et al., 2013), Bilateral filtering (Durand and Dorsey, 2002), Total variation (Goldstein and Osher, 2009), SURELET (Thierry and Florian, 2007), wavelet based Bayes thresholding (Chang et al., 2000), medical image denoising based on soft thresholding using biorthogonal multiscale wavelet transform (Prakash and Khare, 2014) and proposed scheme respectively. The image quality is measured by visual inspection as there is no generally accepted objective way to judge the image quality of a denoised image. There are two criteria widely used in the literature are: (1) visibility of the artifacts and (2) preservation of edge details. The performance of LLSURE method as shown in Fig. 5, is not satisfactory, specially in homogenous regions and near the edges. The method of Bilateral filtering as shown in Fig. 6, provides smoother edge preserved results in homogenous regions. For higher noise level, edge preservation of small detail parts are not satisfactory for clinical purpose. The results of Total Variation (TV) denoising as shown in Fig. 6, give edge preserved smooth denoised images but texture is not as good as for clinical purpose. The results of SURELET, wavelet based denoising using Bayes thresholding and Biorthogonal wavelet thresholding as shown in Figs. 8–10 respectively are providing smoother edge preserved results in homogenous regions. As the noise level increases, Bayes and Biorthogonal wavelet thresholding methods failed to provide the smooth data over the homogenous regions. SURELET also failed to provide satisfactory results on the edges over the higher noise level. The proposed scheme performs several intermediate results using variation and averaging on high frequency coefficients to get final denoised image. The proposed denoising method employs a locally adaptive thresholding where all tetrolet coefficients of each high-frequency subbands are thresholded using the coefficients in their local neighborhoods. It is observed that the results of proposed scheme provide better outcomes for effectively noise reduction and edge preservation of the CT images. Fig. 12 shows the difference between the original and noisy images. Figs. 13–19 show the results as the difference between the original images and the filtered ones for each method where visually it can be observed that proposed scheme gives better outcomes in most of the cases. Table 2 shows MSE, PSNR (in dB) and IQI values of the denoised images relative to their original images for proposed and existing methods. The best values among all the methods are represented in bold. The results shown in Table 2 demonstrate that in most of the cases, the proposed method is superior to all other methods.

5. Conclusions

An alternate post processing approach of iterative method has been proposed to denoise the CT images using locally adaptive thresholding rule in tetrolet domain. Patch wise variance based weighted average gives the strength to get finer details and effective denoising. The proposed method can be implemented very simply and more efficiently than many existing denoising methods. In most of the cases, the MSE, PSNR and IQI values of proposed scheme are better in comparison to existing methods. Apart from MSE, PSNR and IQI, the visual quality of

proposed scheme over the CT images is better in terms of clinically relevant details. Experimental results demonstrate that our proposed method: (i) effectively eliminate the noise in CT images, (ii) preserve the edge and geometrical structures, and (iii) retain clinically relevant details.

References

Abramovitch, F., Sapatinas, T., Silverman, B.W., 1998. Wavelet thresholding via a Bayesian approach. J. Roy Stat. Soc. 60 (4), 725–749.

Aharon, M., Elad, M., Bruckstein, A., 2006. K-SVD: an algorithm for designing overcomplete dictionaries for sparse representation'. IEEE Trans. Signal Process 54, 4311–4322.

Ali, S.H., Sukanesh, R., 2011. An efficient algorithm for denoising MR and CT images using digital curvelet transform. Adv. Exp. Med. Biol. 696, 471–480.

Antoniadis, A., Fan, J., 2001. Regularization of wavelet approximations. J. Am. Stat. Assoc. 96 (455), 939–967.

Beekman, F.J., Kamphuis, C., 2001. Ordered subset reconstruction for X-ray CT. Int. J. Med. Phys. Res. Practice 46, 1835–1844.

Borsdorf, A., Raupach, R., Flohr, T., HorneggerTanaka, J., 2008. Wavelet based noise reduction in CT-images using correlation analysis. IEEE Trans. Med. Imaging 27 (12), 1685–1703.

Buades, A., Coll, B., Morel Song, J.M., 2005. A review of image denoising algorithms, with a new one. SIAM J. Multiscale Model. Simul. 4 (2), 490–530.

Chambolle, A., 2004. An algorithm for total variation minimization and applications. J. Matter Image Visual., J. Roy Stat. Soc. 20 (1), 89–97.

Chang, S.G., Yu, B., Vetterli, M., 2000. Adaptive wavelet thresholding for image denoising and compression. IEEE Trans. Image Process. 9 (9), 1532–1546.

Donoho, D.L., 2010. De-noising by soft-thresholding. IEEE Trans. Inf. Theory 41 (3), 613–627, Signal Process 90(8) pp. 2529–2539, 2010.

Donoho, D.L., Johnstone, I.M., 1994. Ideal spatial adaptation via wavelet shrinkage. Biometrika 81, 425–455.

Durand, F., Dorsey, J., 2002. Fast bilateral filtering for the display of high dynamic range images. ACM Trans. Graphics 21 (3), 257–266.

Fathi, A., Naghsh-Nilchi, A.R., 1989. Efficient image denoising method based on a new adaptive wavelet packet thresholding function. IEEE Trans. Image Process. 21 (9), 3981–3990.

Gao, H.Y., 1998. Wavelet shrinkage denoising using the nonnegative garrote. J. Comput. Graph. Stat. 7 (4), 469–488.

Gao, H.Y., Bruce, A.G., 1997. WaveShrink with firm shrinkage. Stat. Sin. 7, 855–874.

Goldstein, T., Osher, S., 2009. The split Bregman method for L1 regularized problems. SIAM J. Imaging Sci. 2 (2), 323–343.

Gupta, D., Anand, R.S., Tyagi, B., 2014. Despeckling of ultrasound medical images using nonlinear adaptive anisotropic diffusion in nonsubsampled shearlet domain. Biomed. Signal Process. Control 14, 55–65.

Hashemi, S.M., Paul, N.S., Beheshti, S., Cobbold, R.S.C., 2015. Adaptively tuned iterative low dose CT image denoising. Comput. Math. Methods Med.

Jain, P., Tyagi, V., 2015. An adaptive edge-preserving image denoising technique using tetrolet transforms. J. Visual Comput. 31 (5), 657–674.

Jain, P., Tyagi, V., 2015. LAPB: locally adaptive patch-based wavelet domain edge-preserving image denoising. J. Inf. Sci. 294, 164–181.

Krommweh, J., 2010. Tetrolet shrinkage with anisotropic total variation minimization for image approximation. Signal Process. 90 (8), 2529–2539.

Li, K., Zhang, R., 2010. Multiscale wiener filtering method for low-dose CT images. IEEE Biomed. Eng. Inf.s, 428–431.

Mallat, S., 1989. A theory for multiresolution signal decomposition: the wavelet representation. IEEE Trans. Pattern Anal. Mach. Intell. 11 (7), 674–693.

Manduca, A., Yu, L., Trzasko, J.D., Khaylova, N., Kofler, J.M., McCollough, C.M., Fletcher, J.G., 2009. Projection space denoising with bilateral filtering and CT noise modeling for dose reduction in CT. Int. J. Med. Phys. Res. Practice 36 (11), 4911–4919.

Minasyan, S., Astola, J., Egiazarian, K., Guevorkian, D., 2006. Parametric Haar-like transforms in image denoising. IEEE Int. Conf. Image Process., 2629–2632

Motwani, M.C., Gadiya, M.C., Motwani, R.C., Harris, F.C., 2004. Survey of image denoising techniques. In: Proceedings of Global Signal Processing Expo and Conference (GSPx '04), pp. 27–30.

Naimi, H., Adamou-Mitiche, A.B.H., Mitiche, L., 2015. Medical image denoising using dual tree complex thresholding wavelet transform and Wiener filter. J. King Saud Univ.-Comput. Inf. Sci. 27 (1), 40–45.

Prakash, O., Khare, A., 2014. Medical image denoising based on soft thresholding using biorthogonal multiscale wavelet transform. Int. J. Image Graphics 14 (01n02), 1450002.

Qiu, T., Wang, A., Yu, N., Song, A., 2013. LLSURE: local linear surebased edge-preserving image filtering. IEEE Trans. Image Process. 22 (1), 80–90.

Rabbani, H., 2009. Image denoising in steerable pyramid domain based on a local Laplace prior. Pattern Recognit. 42 (9), 2181–2193.

Rabbani, H., Nezafat, R., Gazor, S., 2009. Wavelet-domain medical image denoising using bivariate laplacian mixture model. IEEE Trans. Biomed. Eng. 56 (12), 2826–2837.

Thierry, B., Florian, L., 2007. The SURE-LET approach to image denoising. IEEE Trans. Image Process. 16 (11), 2778–2786.

Vidakovic, B., 1998. Nonlinear wavelet shrinkage with Bayes rules and Bayes factors. J. Am. Stat. Assoc. 93 (441), 173–179.

Zhoubo, Li, Lifeng, Yu., Joshua, D. Trzasko, David, S. Lake, Daniel, J. Blezek, Joel, G. Fletcher, Cynthia, H. McCollough, Manduca, A., 2014. Adaptive nonlocal means filtering based on local noise level for CT denoising. Int. J. Med. Phys. Res. Practice 41 (1), 011908.

Zhu, F., Carpenter, T., Gonzalez, D.R., Atkinson, M., Wardlaw, J., 2012. Computed tomography perfusion imaging denoising using Gaussian process regression. Phys. Med. Biol. 57 (12), N183–N198.